# Towards the self-consistent implementation of active and passive coils for non-linear magnetohydrodynamic simulations of tokamak plasmas

Bachelorarbeit

zur Erlangung des akademischen Grades
Bachelor of Science
im Studiengang SLL-Physik
der Naturwissenschaftlich-Technischen Fakultät II
- Fachrichtung Physik und Mechatronik -
der Universität des Saarlandes

von
Nina Schwarz

Saarbrücken, 2017

Ich versichere hiermit, dass ich die vorliegende Arbeit selbstständig verfasst und keine anderen als die angegebenen Quellen und Hilfsmittel benutzt habe.

Saarbrücken, den ..... .....

Nina Schwarz

## Abstract

ITER is a tokamak, a toroidal fusion reactor, which is currently under construction in the South of France. Fusion devices could play a role in the supply with clean energy in the future. Their working principle is to confine plasma in a limited region of space by magnetic coils at high densities and temperatures to make fusion reactions of two nuclei possible. This is a technically challenging task as the plasma has to be confined for a long enough time to gain sufficient energy.

Tokamak plasmas are disrupted by fast growing instabilities, which not only affect the confinement but also cause damage to the surrounding wall. Namely for ITER it is crucial to find effective methods to mitigate instabilities. One kind of instability, the Edge Localised Modes (ELMs), are hard to control and could significantly decrease the life time of material components. The application of a magnetic perturbation field by coils is one promising mitigation method under research.

Apart from this application, coils play an important role in tokamaks as they not only determine the shape and position of the plasma but also allow to draw conclusions about the current state of the plasma. Simulations help to understand the physical processes in a plasma and allow to make predictions about the behaviour in different fusion reactors. The work of this thesis was done with the non-linear MHD code JOREK which was coupled with STARWALL to model a conductive wall with coils. The task was to work with the extension of STARWALL to model passive and active coils. This implementation has the advantage that it calculates the effect of the magnetic field of the coils more realistically.

First tests with this version of JOREK-STARWALL prove to be promising, as benchmark tests with another MHD code give valid results. Furthermore, we have shown that the magnetic field perturbation is close to the expected values. Future tasks include more thorough testing of the magnetic field penetration in the plasma to explain the deviation from the predicted value.

# Contents

# Abbreviations

| | |
|---|---|
| A | Ampère |
| AUG | ASDEX Upgrade (Tokamak, Germany) |
| DIII-D | Tokamak (USA) |
| ELM | Edge localized mode |
| ITER | International Thermonuclear Experimental Reactor |
| JET | Joint European Torus (Tokamak, UK) |
| PFC | Plasma facing component |
| RMP | Resonant magnetic perturbation |
| $\psi$ | Poloidal Magnetic Flux |
| $\phi$ | Toroidal angle |
| $\varphi$ | Poloidal angle |

# List of Figures



# List of Tables

# 1 Introduction

The aim of fusion research is the development of power plants which harvest energy from nuclear fusion processes. The temperature must be sufficiently high to make the fusion of two nuclei possible, therefore it is called thermonuclear fusion. At these high energies the atoms are completely ionized such that ions and electrons can move separately, forming a plasma [Che15]. One possible method to contain plasma is confinement by magnetic fields as it is done for example in a tokamak where magnets confine the plasma to a toroidal region.

Coils in tokamaks have various purposes, most importantly plasma confinement as well as shape and position control. The main toroidal magnetic field is created by toroidal field coils, while the poloidal magnetic field is created by a toroidal current. This current is induced by a solenoid in the center of the configuration.

In addition to this, there are diagnostic coils that collect information about the plasma by measuring the magnetic flux changes and Error Field coils which are designed to control instabilities.

Instabilities are a major issue in tokamak plasmas, namely in ITER [ITE], the next big step towards the first fusion power plant, currently under construction in France. One kind of instability, the Edge Localized Modes (ELMs), has to be controlled as it can cause serious damage to the walls. A promising mitigation method is the application of resonant magnetic perturbations by so called RMP coils.

In order to make valid predictions for experiments and to better understand the physics of plasmas, simulations are being made which show the time evolution of the plasma.

Some aspects of the plasma dynamics, in particular large scale instabilities, can be described very well in the frame of the magnetohydrodynamic (MHD) equations, a set of partial differential equations which describes the plasma as a fluid and defines the time evolution of the system.

JOREK [Huy07, Cza08] is a non-linear MHD code for toroidal geometries. In the version used for this thesis, it solves a reduced form of the MHD equations with two-fluid and neoclassical extensions [Ora13]. A full MHD version is available as well [Hav16]. JOREK can be coupled [Hoe12] to another code, STARWALL [Mer15], which calculates the effects of a resistive wall. The latter code has recently been extended to include coils in the calculation.

The goal of this bachelor thesis is to contribute to the implementation of coils in STARWALL and JOREK, to its validation, and to carry out first applications of diagnostic and resonant magnetic perturbation coils.

In the following, first an introduction to the physical background of plasma

physics and thermonuclear fusion is given. The structure and characteristics of a tokamak are described in section 2.2 including different kinds of coils and their purpose in section 2.3. Furthermore, Edge Localized Modes are discussed in section 2.4. This is followed by an overview of mitigation methods in section 2.5 for these modes with a focus on RMP coils. In section 2.6, the two codes JOREK and STARWALL are described. The second part of the thesis contains the practical work and its results. Therein, the implementation of coils in STARWALL and JOREK is described in the sections 3.1 and 3.2. Finally, different test cases were calculated to show the validity of the implementation. These include a benchmark test with another MHD code in section 3.3, the interaction of two coils in section 3.4, the analytical calculation of the magnetic flux induced by a circular coil and its comparison to the JOREK results in section 3.5, as well as an RMP case which is compared to a previous simplified implementation in section 3.6.

# 2 Theoretical background

In this section, a theoretical background for the thesis is given. First, the principles of thermonuclear fusion and plasma physics are discussed in section 2.1. Second, the various shapes of fusion reactors are introduced with a focus on the tokamak in section 2.2. Furthermore, different coil types in tokamaks and their use are described in section 2.3 as the practical part deals mainly with the implementation of coils in JOREK and STARWALL. Edge Localized Modes and control mechanisms are introduced in the sections 2.4 and 2.5. Finally, the codes JOREK and STARWALL and their usage are described in section 2.6.

## 2.1 Plasma Physics and Thermonuclear fusion

An important naturally appearing example for fusion is the sun. Without its energy life on earth would not be possible. Different from nuclear fission, two light nuclei are combined to form a bigger nucleus while releasing energy. The information in this section are taken from [Miy06, Wes11, Che15], reference books for plasma physics and tokamaks in particular. To allow the fusion reaction, two protons have to overcome the electromagnetic repulsion, the so called Coulomb wall, in order to combine to a bigger nucleus. This is only possible under certain conditions for density and temperature. Thanks to the quantum mechanical tunnel effect, the required temperature is decreased as protons cross the barrier with a certain probability, even if their energy is not high enough to overcome it. While hydrogen and helium atoms are the main participants in fusion processes on the sun, hydrogen isotopes are used to obtain helium and a neutron in each reaction in laboratory conditions. Pairing Deuterium and Tritium is most promising in terms of reaction rate and and energy output, 17.6 MeV per reaction, which is mainly stored in the neutron.

$$ {}^{2}_{1}\mathrm{D} + {}^{3}_{1}\mathrm{T} \rightarrow {}^{4}_{2}\mathrm{He} + {}^{1}_{0}\mathrm{n} \qquad (17.6\mathrm{MeV}) \tag{1} $$

While Deuterium is abundant in nature, Tritium is extremely scarce and radioactive with a half time life of 12.5 years. However, Tritium can also be produced in a reaction of neutrons with Lithium which is called Tritium breeding.

An important requirement for fusion processes, which are supposed to fuel a power plant, is the ignition condition. This is the point, where the reaction rate is high enough that the heating by $\alpha$-particles created in the reaction is sufficient to balance the energy losses due to radiation and particle loss. The condition can be formulated as

$$ n\tau_E > \frac{12T}{\langle \sigma v \rangle E_\alpha}, \tag{2} $$

where $n\tau_E$ is the product of confinement time and density, $T$ is the temperature, $\langle \sigma v \rangle$ is the reaction rate and $E_\alpha$ is the energy of one $\alpha$-particle.

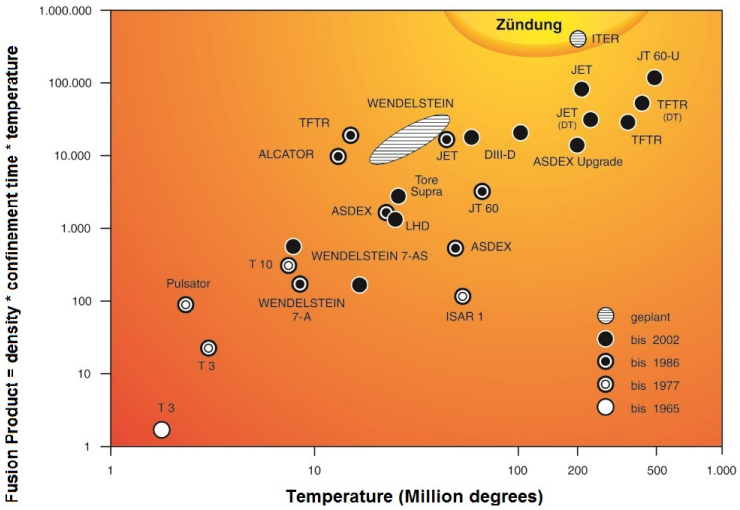


Figure 2.1: The fusion product, the product of density, temperature and confinement time, is an indicator for the ignition condition. The figure above shows the fusion product against temperature in Million degrees Kelvin. In the region on the top, marked in yellow, the ignition condition is fulfilled. In this case, the heating by alpha-particles created in fusion process is sufficient to sustain the plasma. The other marks show how close current and past fusion reactors came to fulfilling the ignition condition while ITER is planned to produce ten times its input energy. (from IPP Bildarchiv ipp.mpg.de, 19.04.2017), modified

The atoms are fully ionised in the plasma state, so that the electrons can move around freely. The motion of charged particles are determined by the Maxwell equations. However, as there is a huge amount of particles, it is impractical to solve the full kinetic equations describing the motion of all particles. Instead, so called moments of the distribution function can be derived of the kinetic equations in order to describe the plasma as a fluid. Together with additional assumptions, the magnetohydrodynamic (MHD) equations are obtained:

$$\frac{\partial \rho}{\partial t} = -\nabla \cdot (\rho \vec{v}) \qquad \text{continuity equation} \qquad (3)$$

$$\rho \left( \frac{\partial \vec{v}}{\partial t} + \vec{v} \cdot \nabla \vec{v} \right) = \vec{v} \times \vec{B} - \nabla p \qquad \text{equation of motion} \qquad (4)$$

$$\nabla \times \vec{B} = \mu_0 \vec{j} \qquad \text{Ampère's law} \qquad (5)$$

$$\nabla \times \vec{E} = \frac{\partial \vec{B}}{\partial t} \qquad \text{induction equation} \qquad (6)$$

$$\nabla \cdot \vec{B} = 0 \qquad \text{Gauss's law of magnetism} \qquad (7)$$

$$\frac{\mathrm{d}}{\mathrm{d}t} \left( p \rho^{-\gamma} \right) = 0 \qquad \text{Adiabatic equation} \qquad (8)$$

The meaning of the variables are listed in table 1. The equations above are the ideal MHD equations, that consider the plasma as a single fluid without resistivity and collisions. In JOREK, a more complicated set of visco-resistive two-fluid equations is solved [Ora13].

Table 1: Variables used in the ideal MHD equations (3)-(8) that describe the plasma as a single fluid with no resistivity and dissipative effects

| variable | physical quantity |
|---|---|
| $\rho$ | mass density |
| $p$ | pressure |
| $\gamma$ | ratio of specific heats |
| $\vec{v}$ | fluid velocity |
| $\vec{j}$ | current density |
| $\vec{B}$ | magnetic field density |
| $\vec{E}$ | electric field strength |

Because of the large temperatures that are required for fusion processes, the plasma cannot be contained by a physical boundary as no material would withstand such conditions undamaged. Thus, another method to confine the plasma has to be found. As the particles are in the plasma state, the solution for thermonuclear fusion is to use magnetic confinement. Different forms have been conceived, among which the two most important ones will be explained in the following section.

## 2.2 Geometries of fusion reactors

In the section above, the requirements for fusion were described. The references [Che15, Igo14, Miy06] contain an overview about the requirements and specifications of plasma reactors, while [Wes11] describes all aspects of tokamaks comprehensively. It is necessary to contain the plasma in a limited region of space to

cross the density and temperature threshold for fusion. The mass in the sun is high enough to confine the particles by gravitation, which is not the case for laboratory plasmas. Possible other methods of confinement are inertial confinement, where the plasma is heated with laser beams, or magnetic confinement.

The latter will be discussed here, as it is the working principle for fusion reactors. When particles are in the plasma state, they react strongly to magnetic and electric fields. Therefore, the idea is to confine them with a magnetic field, as charged particles follow the field lines in a gyrating motion. In most plasma devices, the particles are trapped in a toroidal configuration in which the particles follow the toroidal field lines. If a linear, rather than a toroidal geometry, was chosen there would be significant particle losses at the ends of the device. Because of the combination of several radial particle drifts, namely the $\nabla\vec{B}$, curvature and $\vec{E}\times\vec{B}$ drifts [Che15], a purely toroidal field is not sufficient to confine the particles. To prevent particle losses, the magnetic field must therefore have a poloidal component. Two possible forms of plasma reactors, the stellerator and the tokamak are described below.

### Stellerator and Tokamak

In a stellerator, external coils produce a three dimensional magnetic field which confines the particles in the vacuum vessel. The idea for this device came up in the 1950s by Spitzer in Princeton and since then, various forms of stellerators have been developed. One example is shown in figure 2.2(a) that shows the external coils around the device. This is the stellerator Wendelstein 7-X finished in 2016 in Greifswald which is one of the most advanced working devices. In stellerators some instabilities and in particular disruptions do not occur as there are practically no currents. Also, the device can be used in steady state operation, meaning that one discharge can last up to several hours. Those are the main advantages of this configuration. Because of the complex coil structure and the required precision of the construction, the stellerator research is not as advanced as for tokamaks. Apart from this, the particle losses are still high compared to those of tokamaks. Therefore, it is necessary to optimise the coil configuration to obtain better results. Thanks to improved computational powers, the stellerator can become more important in the future.

The first tokamaks were built in the Soviet Union in the 1950s. Thus, the name has its origin in the Russian words for 'toroidal chamber' and 'magnetic coil'. The shapes of the plasma cross section vary from a circular to a D-form.

Different from the stellerator, the poloidal magnetic field of a tokamak is created mainly by a toroidal current in the plasma as well as by toroidal field coils and its magnitude is ten times lower than the toroidal magnetic field. The toroidal

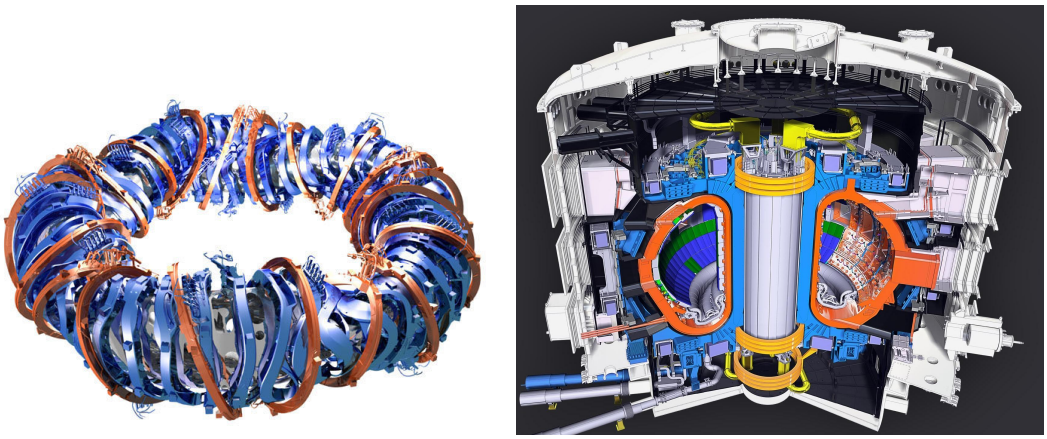

Figure 2.2: Comparison between a tokamak and a stellerator. In stellerators, the poloidal component of the magnetic field is created by the complicated setting of the coils, while it is induced by a toroidal plasma current in tokamaks. (from IPP Bildarchiv http://ipp.mpg.de, 19.04.2017)

plasma current is presently induced mostly by a solenoid in the middle of the torus. Owing to this method, the duration of the discharge is limited as the current in the coil will reach its maximum value at some point. The toroidal magnetic field can have a value of several Tesla and the toroidal current has typically a value of several MA. Current tokamak discharges last several seconds whereas those in ITER are supposed to last about fifteen minutes. The material used in the vacuum vessel, which has to withstand large heat loads and temperatures, consists typically of carbon, Tungsten, Beryllium and steel.

The position in a tokamak is described by a set of flux coordinates $\{\psi, \phi, \theta\}$ which are defined by the surfaces of equal poloidal magnetic flux $\psi$ and two angular variables $\phi$ and $\theta$, the first of which is the toroidal and the latter the poloidal angle. In a normalised system, the outermost flux surface is $\psi_{\mathrm{N}} = 1$ and the flux is defined by:

$$\psi_N = \frac{\psi - \psi_{\mathrm{axis}}}{\psi_{\mathrm{bnd}} - \psi_{\mathrm{axis}}}, \tag{9}$$

where $\psi_{\mathrm{axis}}$ is the magnetic flux on the magnetic axis and $\psi_{\mathrm{bnd}}$ is the magnetic flux on the boundary. Another important concept is the safety factor $q$. It is defined as the ratio between toroidal and poloidal turns of a magnetic field line, when it is traced around the torus. This number is an important factor for plasma stability. When a field line is traced, the safety factor $q$ is given by:

$$q = \frac{\#\,\text{poloidal turns}}{\#\,\text{toroidal turns}} \tag{10}$$

In general, a plasma with a high q at the boundary is more stable. The q-profile depends on the equilibrium conditions and the form of the plasma. Flux surfaces

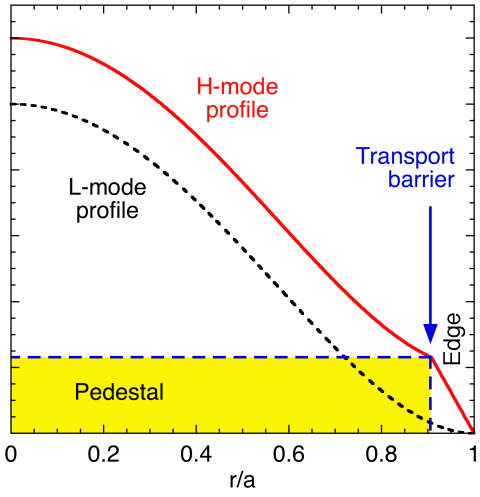


Figure 2.3: When the heating power exceeds a certain limit, the plasma changes to a higher confinement mode, the H-mode. In contrast, the lower confinement mode is called the L-mode. The pressure profile of a tokamak plasma in L-mode and H-mode are shown in this figure. In H-mode, the pressure seems to be put on a pedestal which leads to a steeper pressure gradient at the and reduced edge transport. Therefore, the H-mode creates an edge transport barrier which results in better confinement. (from fusionwiki `http://fusionwiki.ciemat.es/wiki/Pedestal`, 19.04.2017)

with rational values of q are prone to plasma instabilities.

The tokamak can be operated in a high confinement mode called H-mode. This state can be achieved more easily when the plasma shape is in a so called X-point configuration. Both terms are explained in the following section.

### H-Mode and X-point configuration

During a discharge in the tokamak ASDEX in Garching in the 1980s, it was observed that the plasma suddenly had a twice as good confinement as before. This operation mode was subsequently named the 'H-mode' due to the high confinement, whereas the operation mode at lower confinement is called the 'L-mode'. When the heating power exceeds a certain threshold, the plasma changes from L- to H-mode. The H-mode is characterised by a higher pressure which looks like it is put on a pedestal in comparison to the L-mode pressure profile. This results in a higher pressure throughout the plasma and a steeper pressure gradient at the edge. The higher confinement is due to the large pressure gradient, which reduces the edge transport by creating a so called edge transport barrier. However, this caused a new kind of MHD instability, the Edge Localized Modes, that is explained further below.

It is easier to reach the H-mode when the plasma is in a so called X-point

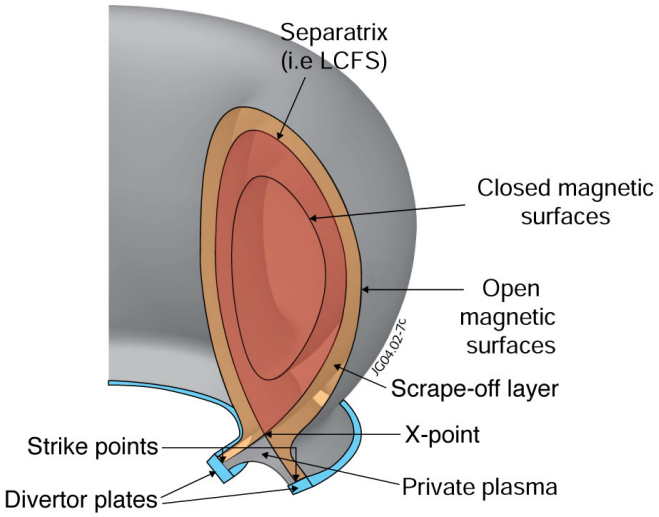


Figure 2.4: Shape of the plasma cross section in X-point configuration. The separatrix is defined as the last closed flux surface. The flux surfaces inside the plasma are closed while the ones outside are open and can intersect with the wall, for example. The poloidal flux is zero at the X-point. The divertors are designed to withstand high heat loads as the plasma is directed towards them. (from Euro-Fusion https://www.euro-fusion.org, 19.04.2017)

configuration. The shape of the plasma can be seen in figure 2.4. The separatrix represents the last closed magnetic flux surface which separates the closed flux surfaces within the confined plasma from the open flux surfaces. Outside of the separatrix pressure and density drop rapidly. A plasma can have several X-points where the poloidal magnetic field is zero. In the places where the plasma hits the wall, there are divertors installed which are designed to take up large heat loads. A point where the plasma touches the divertor is called a strike point.

Inside and outside of the vacuum vessel there are several coils installed. As different coil types are important for the practical part of the thesis, their geometry and purpose is described in the following section.

## 2.3 Coils in tokamaks and their purpose

Coil sets in various forms and for different purposes can be found in a tokamak as figure 2.5 shows. The books [Dol13, Boy03] were used for this summary about coils in tokamaks.

The first kind of coils is responsible for the confinement of the particles in the torus. Among those there are the toroidal field coils which create the toroidal field component which is the reason the particles move in toroidal direction. As mentioned above, outward drifts of particles have to be compensated by a

poloidal field which is induced by the toroidal current. This toroidal current is mostly created by the central solenoid in the center of the torus. The toroidal magnetic field is about one order in magnitude bigger than the poloidal field.

Second, there are several poloidal field (PF) coils which control the plasma shape as well as its vertical position and contribute to the poloidal magnetic field. They have a toroidal symmetry and are placed on different heights and distances around the plasma.

Third, there are Error Field coils which create a small magnetic error field with the aim to control instabilities. The perturbation is small with respect to the magnetic field in the plasma. One kind of error field coil creates resonant magnetic perturbations (RMPs) which can result in magnetic islands in the plasma. Their function and working principle will be explained more in detail below.

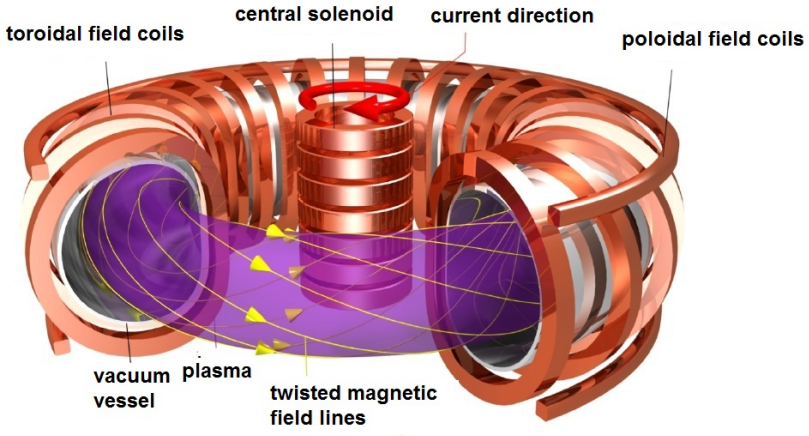


Figure 2.5: Cross section of a tokamak with different coil sets that fulfill various functions. The toroidal current, which is essential for plasma confinement, is induced by the central solenoid in the center of the configuration. The toroidal magnetic field is created by toroidal field coils while poloidal field coils control the plasma shape and position. Error field coils are used to create small magnetic perturbations to control instabilities. This figure does not show diagnostic coils which are passive elements used for analysis of the plasma. (from IPP Bildarchiv http://ipp.mpg.de, modified, 19.04.2017)

Finally, apart from active coils that modify the plasma, there are passive coils, in which no external voltage is set. Instead, they pick up the magnetic flux from the plasma which induces a current. The current is induced according to Faraday's law:

$$\oint \vec{E} \cdot \mathrm{d}\vec{l} = -\oint \frac{\partial \vec{B}}{\partial t} \cdot \mathrm{d}\vec{S}, \tag{11}$$

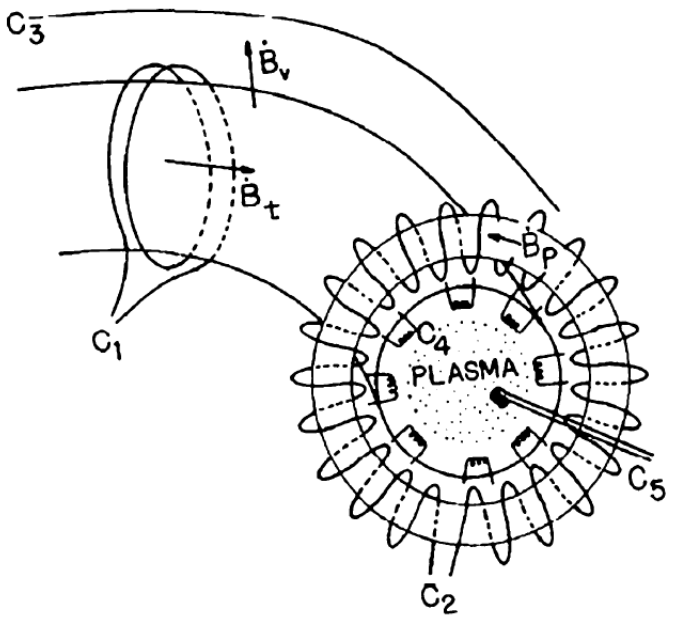


Figure 2.6: The figure shows possible orientations for magnetic flux coils around the plasma. Different orientations and shapes of the coils allow to measure different components of the magnetic flux, as only changes normal to the coil surface induce a current. A wire in the horizontal plane measures the flux changes in vertical direction, while a coil in the poloidal plane measures the changes in toroidal direction. In order to measure poloidal flux changes the coil has to be wound around the plasma as coil C2 in this figure. This configuration is called a Rogowski loop. Mirnov coils (C4) are put close to the plasma where they can measure magnetic perturbations in the plasma edge. (from [Dol13, p. 523])

where $\vec{l}$ is the line element of the coils and $\vec{E}$ is the electrical field, $\vec{S}$ is the surface of the coil and $\vec{B}$ the magnetic field.

When considering a small loop, the right side simplifies to the product of the coil surface area and the normal component of the magnetic field to the coil area. The left side is equal to the voltage induced in the loop. Thus, we acquire equation (12), that tells us that the induced voltage $V$ in the coil depends only on the changes of the magnetic field component $B_\mathrm{n}$ normal to the coil surface $A$.

$$V = A\frac{\partial B_n}{\partial t} \tag{12}$$

According to this equation the orientation of the magnetic flux coil determines the component of the magnetic flux change that is measured. Figure 2.6 shows possible configuration for the pickup coils.

A wire in the poloidal plane can measure the toroidal flux changes. A coil which is wound around the poloidal cross section, like coil C2 in figure 2.6, is

called Rogowski loop and measures the poloidal magnetic field, while the toroidal coil (C3) measures vertical flux changes. A set of coils that is oriented as the C4 coils in the figure is called Mirnov coils which are used to determine perturbations of the poloidal magnetic field in the plasma edge. The information can help to determine the plasma shape and position as well as the mode number of plasma instabilities as it has been done for example in the references [Min16, Min].

## 2.4 Edge Localized Modes (ELMs)

Various instabilities can occur in tokamak plasmas which have to be controlled if they become unstable. This thesis will focus on the so called Edge Localized Modes (ELMs) that are a main issue for ITER. The references [Igo14, Lan13, Zoh96] give an overview about the current understanding about the physical background and a description of the ELMs occurring in experiments.

After the H-mode was discovered in tokamaks, a new kind of instability occurred which can periodically reduce the plasma energy by up to 20 % on a very short time scale. When such a large amount of high energy particles is suddenly expulsed from the plasma, it can cause serious damage to the plasma facing components (PFCs). In current devices, the components can take up the heat, but an extrapolation to ITER shows that the energy would surpass the $0.5\,\mathrm{MJ/m^2}$ energy limit on the divertor [Lan13]. In this section the phenomenology of the different ELM types is described, afterwards the physics behind them is explained. Finally, different ELM mitigation and suppression techniques are discussed.

Three types of ELMs can be distinguished:

- The type I ELMs describes an ELM phase during which large amounts of energy burst out of the plasma at a moderate frequency of 10-100 Hz. During one ELM up to 20% of the pedestal energy is lost. The frequency increases with the heating power.

- The type II ELMs occur in strongly shaped plasmas at high density. The energy per ELM is lower than during a type I phase which still guarantees good confinement while controlling the impurities in the confined region. They are also called grassy ELMs which occur only at specific conditions that are hard to maintain.

- The type III ELMs are also called small ELMs, and occur at a high frequency and low amplitude. The frequency decreases with increasing heating power. The energy transport through the edge transport barrier is rather high which leads to a lower confinement.

While type I ELMs have to be avoided to prevent material damage, a type III ELM regime also shows positive effects on the plasma like impurity exhaust. Thus, it is necessary to either suppress ELMs completely or to maintain a type III ELM regime.

By looking at the conditions under which ELMs occur, it is possible to learn more about them. ELMs occur at the peeling-ballooning stability limit of the MHD theory and depend mainly on the edge current density and the pressure gradient at the edge.

Peeling modes are resistive instabilities, which appear at the resonant surfaces where the safety factor $q = m/n$ is a rational number. They are driven by the edge current density $\vec{j}_{\text{edge}}$. The pressure gradient $\nabla p$ can act stabilising or destabilising depending on other plasma parameters.

Ballooning modes are caused the curvature of the tokamak. The field line curvature on the high field side at the inner side of the torus has stabilising effects, while the one on the low field side on the outboard side of the torus act destabilising. Low $\nabla p$ scenarios are ballooning stable, as the good curvature effects on the high field side prevail, while there can be instabilities localised at the outboard side of the plasma for higher pressure gradients. This instability is therefore driven by the pressure gradient.

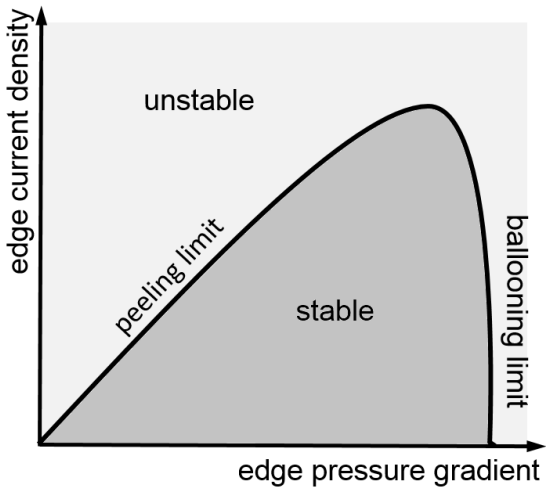


Figure 2.7: The stable regions of the peeling and ballooning modes are shown. Peeling modes occur at high edge current densities $\vec{j}_{\text{edge}}$, while ballooning modes are unstable for high pressure gradients $\nabla p$. They can couple together to peeling-ballooning modes which decreases the area of the stable region. Especially when operated in H-Mode the plasma parameters are close to the peeling-ballooning stability limit. (Recreated from [Igo14, p. 151])

In summary, the peeling mode is unstable for high edge current densities while the ballooning mode is unstable for high pressure gradients. In H-mode plasmas

both values are typically high so that both modes can exist at the same time and couple to a peeling-ballooning mode, so that they occur in formerly stable situations. Figure 2.7 shows the stable and unstable regions of the peeling and the ballooning mode in dependence of the edge current density and the pressure gradient. As ELMs occur when the stability limit of the peeling-ballooning mode is reached, they can be identified as those instabilities.

One ELM cycle can be divided into the following steps. When the plasma enters the H-mode the pedestal pressure and current density build up. The peeling mode is stable at this point. The pressure gradient increases until it reaches the stability limit of the ballooning mode. At this point, a toroidal current called bootstrap current is induced. This additional current results in a crash and the plasma returns to the stable region at lower density and energy until the pressure crosses the stability limit again.

Possible mitigation methods will be introduced in the following section.

## 2.5 ELM mitigation techniques

It is expected that a control mechanism has to be developed in order to prevent serious damage on the divertor and the PFC during an ELM crash. Different approaches have been developed to obtain this goal and are described in detail in the refernces [Lan13, Igo14]. First, the plasma can be maintained at conditions below the instability threshold. Meaning that $\nabla p$ and $\vec{j}_{\mathrm{edge}}$ remain high but still are under the stability limit of the peeling-ballooning mode.

Another method is to trigger a small ELMs before the pedestal top is reached. Thus, the ELM frequency increases and the energy $\Delta W_{\mathrm{ELM}}$ expelled during each crash is lower. The dependence of the ELM energy and the inverse of the frequency frequency $\Delta W_{\mathrm{ELM}} \propto 1/f_{\mathrm{ELM}}$ was found in experiments and seems to hold for different devices see [Lan13]. As the ELM frequency $f_{\mathrm{ELM}}$ is controlled, this technique is called 'ELM pacing'. The advantage of this method is the reduction of the peak heat load on the divertor while the positive effects of the ELMs in terms of impurity transport remain. Techniques that have been conceived and tested include radiation dispersion, vertical kicks, injection of hydrogen pellets and the application of resonant magnetic field perturbations.

The aim of radiation dispersion is to disperse the energy before the the plasma facing components are hit instead of preventing an ELM crash. This is done by impurity seeding which radiate the energy. However, this results in a deterioration of confinement and only works effectively for small ELMs.

One example for an ELM pacing method are vertical kicks. There are already several poloidal field coils which are used to control the vertical position of the

plasma. They can be used to create a small vertical plasma displacement. A shift of about 1 cm is necessary to trigger an ELM. The frequency of the ELMs follows the frequency of the kicks. Like this, it is possible to increase the ELM frequency to reduce the energy per ELM. This method has already been applied in JET, AUG and NSTX for example. In [AS17] the application with STARWALL is explained and further simulation with JOREK-STARWALL are planned.

Another approach is the injection of cold hydrogen pellets to trigger an ELM. They have a size of several millimetres and can in principle be injected from any side of the plasma. It was observed that the triggering works at any point of the ELM cycle. About 1 % of the pellet is absorbed in the plasma providing additional fuelling. The ELM is triggered when the pellet reaches the separatrix. Thus the inner plasma is not perturbed.

A promising approach is ELM control by resonant magnetic perturbations (RMPs). External RMP coils apply a small magnetic perturbation on the plasma edge which creates magnetic islands on the rational surfaces at places where the safety factor $q$ is a rational number. The islands are created by a tearing and reconnection of the magnetic field lines as can be seen in figure 2.8. The laminar structure between the islands is conserved as long as the islands are separated. When the islands grow they get closer to each other until they finally overlap to create an ergodic zone. The magnetic field lines in this area do not remain on the magnetic surface but come arbitrarily close to every point in the zone. The ergodicity enhances the particle and heat transport in the edge layer, while the plasma response to the perturbation shields the inner plasma from the external field. Thus, only the edge plasma is affected by the perturbation.

The increased transport through the edge transport barrier leads to a so called density pump out, which is a significant reduction of the pedestal density and lowers the density of the whole plasma. Apart from this, the plasma rotation is slowed down and the ion temperature increases.

Both complete ELM suppression and mitigation can be achieved, as it has already been shown in various experiments including ASDEX Upgrade [Sut11], JET [Lia10] or DIII-D [Eva04]. The effect of the RMPs depends also on the shape of the plasma, its rotation and the collisionality. The mitigation is similar to a type III ELM regime with frequent, but weaker ELMs. Altogether, the application of resonant magnetic perturbations leads to a degraded confinement of up to 10 % due to density reduction. The loss of particles can only be partly compensated by injection of pellets.

One possible form of coils, currently installed in Asdex Upgrade, can be seen in figure 2.9 which consists of 16 coils in total with half on the upper row and the other half on the lower one. The current of each coil can be set individually and

a phase difference between the upper and the lower coil set is usually applied in the experiment. This phase difference influences the amount of ergodisation in the edge which leads to different effects on the edge transport [Ora17].

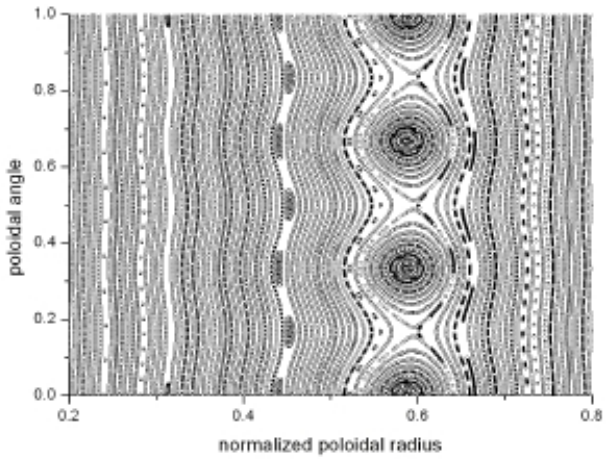


Figure 2.8: Error field coils create magnetic islands on the rational surfaces of the plasma where the safety factor is a rational number. These perturbations are called resonant magnetic perturbations (RMP). When the magnetic islands are large enough to overlap, they create an ergodic zone in the plasma edge which weakens the edge transport barrier and decreases the plasma density. They can mitigate ELMs or suppress them completely. (from IPP Bildarchiv `http://ipp.mpg`, 19.04.2017)

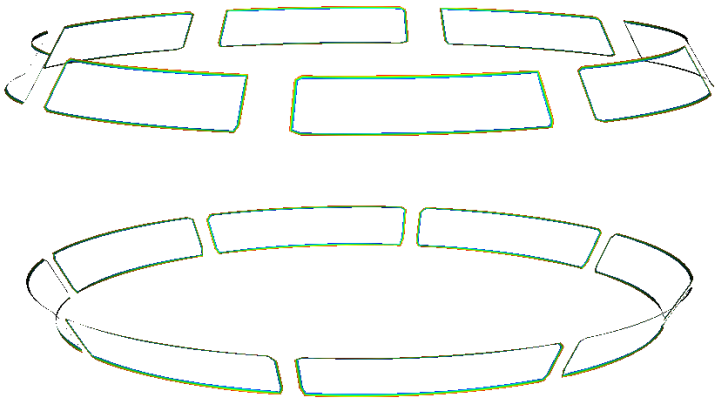

Figure 2.9: Configuration of RMP (resonant magnetic perturbation) coils in ASDEX Upgrade. RMP coils cause a small perturbation of the magnetic field in the outer region of the plasma which creates magnetic islads in the edge. An overlap of these islands result in an ergodic layer with enhanced particle and heat transport through the edge transport barrier. Due to this, the plasma stays peeling-ballooning stable region. (Own representation)

Even if this method looks promising, there still remain open issues. The complete physical explanation of the effect of RMPs is up to date not fully understood. In particular, the role of ergodisation and magnetic islands remains an open question. Furthermore, the plasma response to the magnetic perturbation have to be taken into account as this can have both screening and amplifying effects on the plasma, which make them hard to predict. With regard to ITER, extrapolations have already been made to determine an ideal RMP profile. This method and pellet injection are the techniques that will be used to control ELMs in ITER.

However, further experiments and simulations are necessary, to make reliable predictions. This thesis describes one step to a more realistic handling of coils in simulations, which helps to better understand the effect of RMPs on the plasma.

## 2.6 JOREK and STARWALL codes

JOREK [Huy07, Cza08] is a non-linear MHD code which solves the MHD equations in both the reduced [Fra15] and the full form [Hav16]. In this thesis only the reduced models of the JOREK code are used. The reduced model simplifies the equations by taking into account geometrical effects in a torus. Depending on the JOREK model used, two-fluid and neoclassical effects can be taken into account.

The plasma is discretised in the poloidal plane using the finite element method with bicubic Bézier elements [Cza08]. An example of a grid in the poloidal plane is shown in figure 2.10, where the number of grid points in a double X-point configuration was reduced to show the structure. The toroidal modes are considered by a decomposition in Fourier harmonics. First, the axisymmetric equilibrium is calculated by solving the Grad-Shafranov equation which determines the plasma equilibrium on an initial grid. From this the magnetic flux surface aligned grid is constructed. Afterwards, the time evolution of the system is computed using fully implicit time stepping and more Fourier harmonics can be added to see non-axisymmetric effects. The code is parallelised with OpenMP and MPI.

STARWALL [Mer15] calculates the effect of a conducting wall on the plasma by imposing natural boundary conditions on the boundary of the JOREK calculation domain. Namely, the tangential component of the magnetic field has to be continuous at the boundary. The coupling of the two codes is described in [Hoe12]. Without STARWALL, JOREK has fixed Dirichlet boundary conditions. In contrast, a simulation together with STARWALL is called a freeboundary computation. Fixed boundary conditions correspond to a ideally conducting wall, while freeboundary computations can have a more realistic resistive wall.

The wall is discretised into thin triangles with an effective resistivity of $\eta_W/d_W$

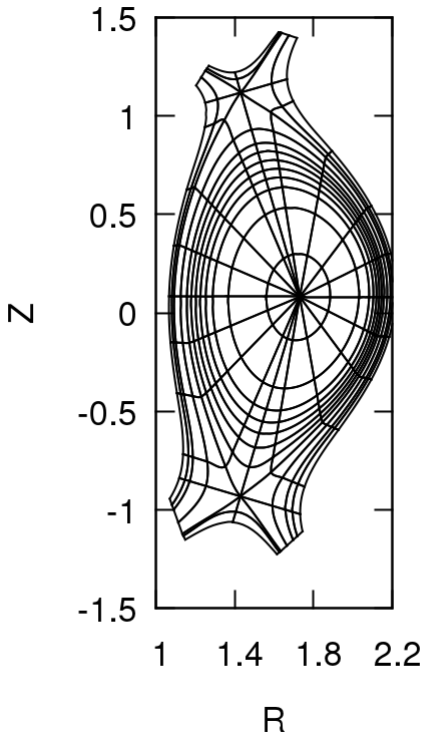


Figure 2.10: The poloidal cross section of the plasma is discretised by bicubic Bézier elements, while the toroidal decomposition is done in Fourier harmonics. Various types of plasma shapes can be represented with this method, from circular to plasmas with one or more X-points. This figure shows an example with two X-points. The number of points was decreased to make the shape better visible. (Own representation)

with the wall resistivity $\eta_W$ and the wall thickness $d_W$. The effect of a unit magnetic perturbation on the JOREK boundary induces a certain current in the wall. STARWALL then calculates the vacuum magnetic field which is used as the boundary condition as its tangential component has to be continuous on the JOREK calculation boundary. The wall effects are handed to JOREK in the form of the so called response matrices where they are then used to calculate the tangential magnetic field on the boundary during the simulation.

At this point, the effect of external coils can only be taken into account by imposing their magnetic field on the boundary as a fixed boundary condition. Thus, implementing coils into STARWALL would offer new possibilities to make more reliable predictions by calculating both coil and wall effects with natural boundary conditions. The task for this thesis is to continue with the implementation of coils in STARWALL and to test the validity of the results. The details follow in the next section.

# 3 Coils in JOREK-STARWALL

The practical tasks of the bachelor thesis include the implementation of a new coil type in STARWALL in section 3.1 and the adaption of JOREK for coils in section 3.2. The results obtained with those modifications have to be verified and checked for consistency. The STARWALL code without coils is benchmarked by comparison with another MHD code in section 3.3. The correct interaction of two coils was verified by placing two current loops close to each other in section 3.4 and the magnetic field produced by active coils is compared to its analytical value in section 3.5. In the end, an RMP case is calculated and compared to a fixed boundary calculation with RMP coils in section 3.6.

## 3.1 Implementation of coils in STARWALL

The implementation of coils in STARWALL requires a discretisation into triangles as it has already been done for the wall. For simplicity, the coils are considered as two dimensional objects with negligible width. The coils are treated differently depending on their geometrical description and their physical meaning. In terms of geometry, axisymmetric coils and so called 'general thin' coils can be distinguished in STARWALL. The implementation of axisymmetric coils has already been implemented and is not the topic of this thesis. Instead the treatment of general thin coils was incorporated in the code. Those coils can have an arbitrary shape and can be treated when their coordinates are given. All coil types share the variables resistivity, number of turns and length.

Triangles for this coil type are created by a a list of points tracing the form of the coil. Additionally, a width has to be set. In figure 3.1 the steps from the original points to the final triangles are shown. First, the coil information including the coordinates of the points are read into STARWALL. From each input point, two band points are constructed at a given length representing the boundaries of the 'triangle band'. The position of the band points are calculated with the following formula where $\vec{r}$ is the vector from the center of the coil to the original point and $\vec{dr}$ is the vector from the precedent point to the following one.

$$\vec{P}_{\pm} = \vec{r} \pm \text{width} \frac{\vec{r} \times \left( \vec{r} \times \vec{dr} \right)}{|\vec{r}|^2 |\vec{dr}|} \tag{13}$$

## 3.2 Implementation of coils in JOREK

As explained in section 2.6 the STARWALL information is handed to JOREK via so called response matrices. The effect of the coil and wall current is taken

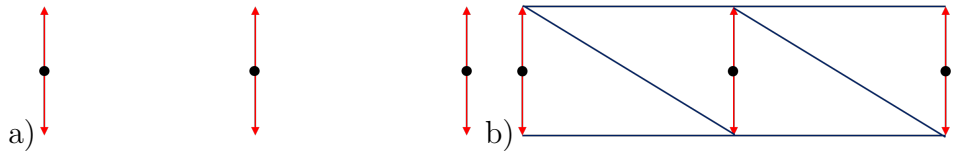


Figure 3.1: The original points are given to STARWALL via an input file. In the next step the center of the coil is calculated, from which the band points of figure a) are constructed. These bands are then divided into triangles as can be seen in figure b). (Own representation)

into account by the continuity of the tangential magnetic field which is imposed by a natural boundary condition as described in section 2.6. As the dynamics of the plasma induce currents in the conducting structures these currents have to be updated at each time step.

The coils in the experiment and JOREK can act as passive or active components. Active coils can be held at constant current or follow a given current profile like for example a sinus function. A voltage $U$ treated as a current source $I$ with the current $I = U/R$ where $R$ is the coil resistance. At the current stage, the current profile is given in an external file where at each time step the value for each coil is given.

Passive coils are used for diagnostic purposes. As explained in section 2.3, the orientation of the coil determines which component of the magnetic flux change is observed. The current is written out after each time step to allow for a virtual measurement of components of the magnetic field vector like in the experiment.

In the following sections, different test cases are carried out and described.

## 3.3 Benchmark of STARWALL without coils

In order to make sure that the modified version of STARWALL and JOREK is consistent, we compare the results with a linear MHD code named CASTOR_FLOW (in the following CASTOR).

First, a simple test case is set up. This consists of a circular plasma with a large aspect ratio with a major radius of 10 m and a small radius of 1 m. The physical parameters are chosen such that the plasma develops a $m/n = 2/1$ tearing mode as it can be seen in figure 3.2. This mode causes a tearing and reconnecting of the magnetic field lines, thus the name. The poloidal mode number $m = 2$ can be seen in the periodicity of the edge current. The codes are compared to each other via the linear growth rate of the tearing mode instability. The growth rate is defined as the logarithm energy difference of the instability between two time steps as:

$$\gamma = \frac{ln\,(E_2/E_1)}{t_2 - t_1} \tag{14}$$

As STARWALL is used to consider the effect of the wall, it is a freeboundary computation. The STARWALL response in this case is calculated for an ideal wall, to stabilise the plasma, without coils. The wall cross section is circular with a radius varying between 1.01 m and 5.0 m, while the radius of the plasma is 1 m.

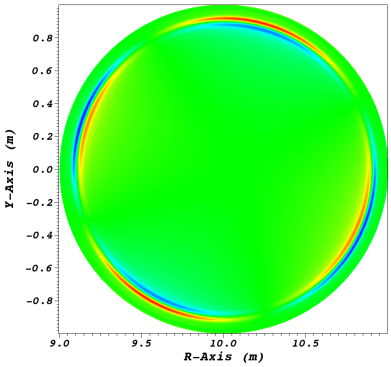


Figure 3.2: The first benchmark tests is carried out in a circular plasma with large aspect ratio in JOREK and another MHD code, CASTOR_FLOW. The conditions are chosen so that a 2/1 tearing mode occurs at the edge as shown in the figure of the current perturbation. The wall is set at different distances to the wall and the resolution of the plasma and the wall is varied in the testcases. The growth rates of the tearing mode are calculated in the codes and compared to each other. (Own representation)

Before comparing the growth rates of JOREK and CASTOR, it is necessary to show that they are converged. For this, they were calculated at different resolutions of the plasma and the wall. In particular, the number of grid points of the plasma and the wall were independently changed over a range of values. Table 2 shows the growth rates for various resolutions. For most of the parameters, a change of their value does not have considerable effects on the growth rate, which means the result is converged. However, as the number of toroidal wall elements, nwv, had a large impact on the growth rate, we had to show that the growth rates are converged at the resolution that is used for the comparison with CASTOR. In figure 3.3, we see that the growth rate converges quickly above a certain value. For the comparison with CASTOR_Flow, 128 and 48 toroidal plasma elements were used for the wall distances of 0.01 and 0.1 respectively. At those values, the growth rate is converged so that the comparison with CASTOR is possible.

The growth rates are calculated with both codes and converted to SI units to compare them. The results can be seen in figure 3.4.

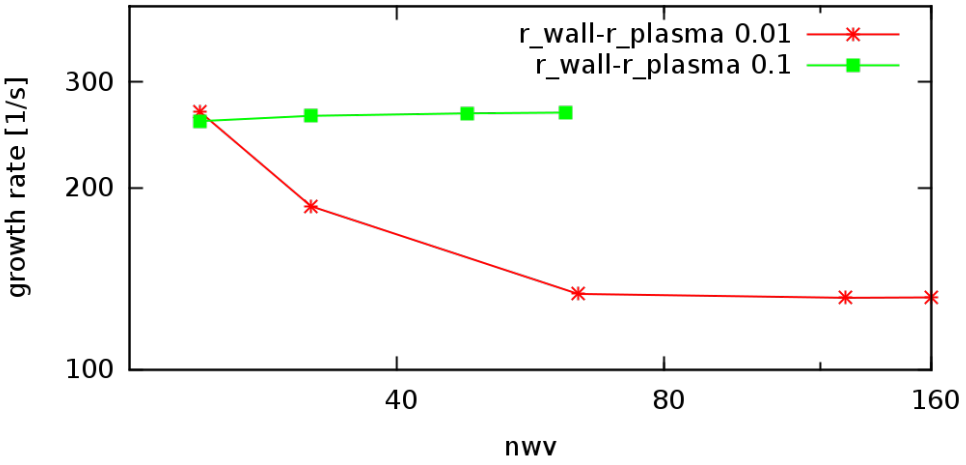


Figure 3.3: The number of wall grid points in toroidal direction (nwv) has a large effect on the growth rates. Because of this $\gamma$ is calculated at a range of values of nwv at a distance of 0.01 and 0.1 m from the plasma. The value for the reference case is 128 at $r_{wall}$-$r_{plasma}$ = 1.01 m and 48 at $r_{wall}$-$r_{plasma}$ = 1.1 m. In the graph it can be seen that the growth rate is converged for those resolutions. (Own representation)

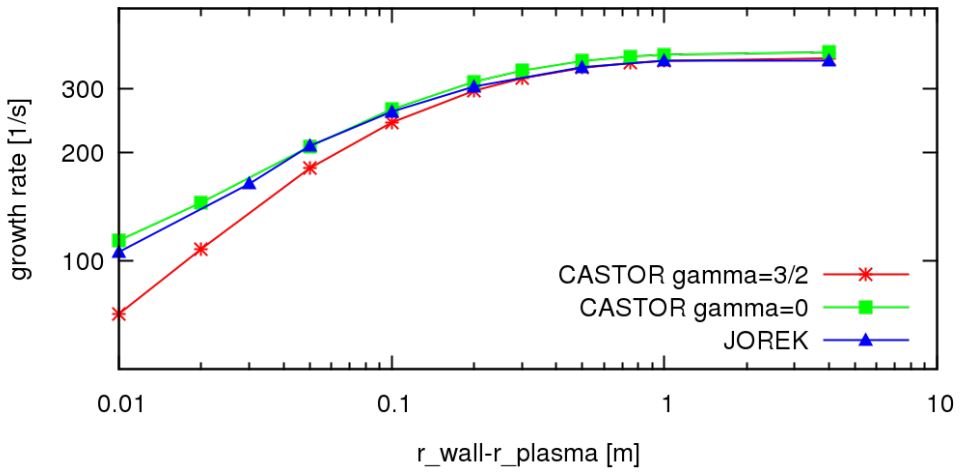


Figure 3.4: The growth rates of the tearing mode were calculated with both JOREK and CASTOR_FLOW for different distances between the wall and the plasma $r_{wall}$-$r_{plasma}$. At the no wall limit, with a wall far from the plasma, the growth rate converge to the same value. For a close wall the values do not fit perfectly due to the partiaal compressibility of the JOREK reduced MHD model. (Own representation)

At the ideal wall limit of a very distant wall, the growth rates converge to the same value. However, when the wall is closer to the plasma, the results deviate. The ratio of specific heats $\gamma$ in CASTOR can be set so that the plasma is considered as either incompressible ($\gamma = 0$) or fully compressible, while the reduced MHD model in JOREK corresponds to a plasma only partly compressible.

The growth rates of JOREK lie in between those versions of CASTOR, suggesting that the different compressibilities are responsible for the deviation.

More comprehensive comparisons including different plasma and wall resistivities will be done in future. As the results for JOREK-STARWALL without coils look promising, we continue with the first coil tests. First, we are going to look at the interaction of two coils.

Table 2: Values of the energy growth rate of the tearing mode for different distances to the wall and different resolutions. These growth rates were calculated with JOREK and compared to the CASTOR values. The parameters ntheta, npoints, nv, nwu and nwv correspond to number of grid points in either the wall or the plasma in a certain direction. The parameters that were used for the benchmark with CASTOR are marked in grey. The resolution was varied for the distances $r_{wall}$-$r_{plasma}$=0.1 and 0.01 to show that the growth rate does not change significantly which tells us that they are converged.

| $r_{wall}$-$r_{plasma}$ | ntheta | npoints | nv | nwu | nwv | growth rate [1/s] |
|---|---|---|---|---|---|---|
| | 16 | 10 | 128 | 128 | 128 | 131.5 |
| | 24 | 10 | 128 | 128 | 128 | 131.7 |
| | 16 | 8 | 128 | 128 | 128 | 131.6 |
| | 16 | 10 | 64 | 128 | 128 | 132.8 |
| 0.01 | 16 | 10 | 128 | 64 | 128 | 130.0 |
| | 16 | 10 | 128 | 128 | 24 | 267.2 |
| | 16 | 10 | 128 | 128 | 32 | 186.6 |
| | 16 | 10 | 128 | 128 | 64 | 133.5 |
| | 16 | 10 | 128 | 128 | 160 | 131.8 |
| 0.03 | 16 | 10 | 92 | 92 | 92 | 177.4 |
| 0.05 | 16 | 10 | 64 | 64 | 64 | 208.2 |
| | 16 | 10 | 48 | 48 | 48 | 265.9 |
| | 24 | 10 | 48 | 48 | 48 | 266.4 |
| | 16 | 8 | 48 | 48 | 48 | 265.5 |
| | 16 | 10 | 24 | 48 | 48 | 268.3 |
| 0.1 | 16 | 10 | 48 | 24 | 48 | 266.9 |
| | 16 | 10 | 48 | 48 | 8 | 346.9 |
| | 16 | 10 | 48 | 48 | 12 | 309.8 |
| | 16 | 10 | 48 | 48 | 24 | 258.3 |
| | 16 | 10 | 48 | 48 | 24 | 263.5 |
| 0.2 | 16 | 10 | 32 | 32 | 32 | 303.8 |
| 0.5 | 16 | 10 | 32 | 32 | 32 | 343.9 |
| 1.0 | 16 | 10 | 32 | 32 | 32 | 357.8 |
| 4.0 | 16 | 10 | 32 | 32 | 32 | 357.8 |

## 3.4 Interaction of two coils

This benchmark test shows that first, an active coil creates the correct magnetic flux and second, a varying magnetic flux induces the correct current in a passive coil. For this, two wire loops facing the same direction are constructed, one of which is handled as an active coil with high resistance and imposed voltage while the other is a passive diagnostic coil with a lower resistance.

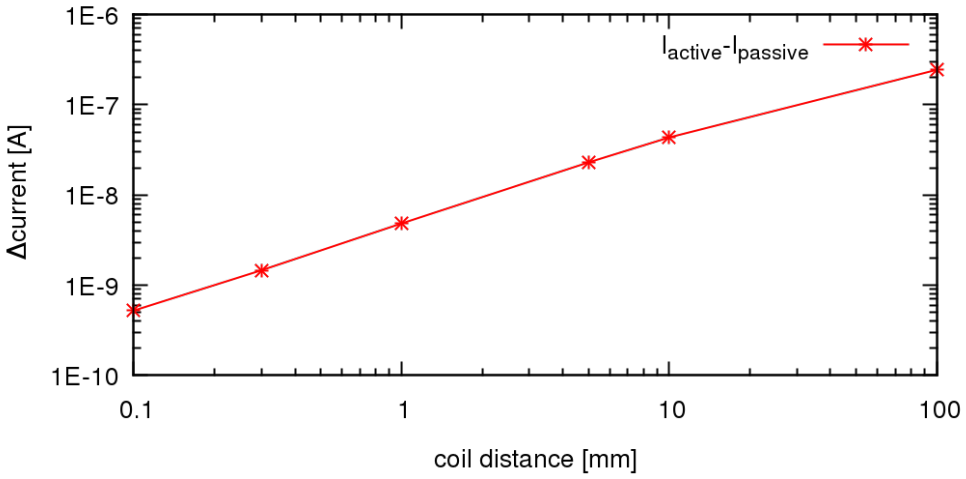


Figure 3.5: Two circular current loops are placed close to each other. A sinusoidal current is imposed in one of them, while the other acts as a passive diagnostic coil. The goal is to see that the currents are equal to another. The difference between the coil currents at the maximum of the sinus function is plotted against the distance between the coils. With decreasing distance the current in the passive coil converges to the imposed value of the active coil. (Own representation)

When the coils are located close enough to each other, the magnetic flux produced by the active coil flows through the whole area of the passive coil inducing the same current. Therefore, the distance is varied from 100 mm to 0.1 mm to see whether the induced current converges to the imposed one in the active component. A sinusoidal current is imposed in the first coil with an amplitude of 1 A. In figure 3.5, the difference of currents at the maximum of the active coil current is plotted against the distance between the loops on a logarithmic scale. The current in the diagnostic coil converges to the imposed value in the active component. This allows the conclusion, that the interaction of two coils is successfully implemented in STARWALL.

Now, it remains to verify whether the interaction between coils and plasma is correct. Therefore, the following section will deswe are going to look at the penetration of the magnetic field in the plasma in the following section.

## 3.5 Comparison between the analytical and calculated magnetic field of a single coil

The magnetic field of a coil can be calculated analytically using the Biot-Savart law. For a simple current loop, a closed analytical expression can be derived as it is done for example in reference [Sim01]. In this case, we will look at the vector potential of a current loop with radius $a$ which is also given in the paper as in the following equation. In the coordinate system of the coil, the origin lies in the center of the loop and the coil in the xy-plane. Only the poloidal component is important as the others cancel each other.

$$\begin{aligned} A_\varphi &= \frac{\mu_0 I a}{4\pi} \int_0^{2\pi} \frac{cos\varphi' d\varphi'}{\sqrt{a^2 + r^2 - 2ar\sin\theta}} \\ &= \frac{\mu_0}{4\pi} \frac{4Ia}{\sqrt{a^2 + r^2 + 2ar\sin\theta}} \left[ \frac{(2-k^2))K\left(k^2\right) - 2E\left(k^2\right)}{k^2} \right] \end{aligned} \tag{15}$$

$A_\varphi$ is the poloidal component of the vector potential, $\mu_0$ the permittivity constant, $I$ the coil current, $r$ the distance to the observation point and $\theta$ the azimuthal angle. The integral of the loop results in the elliptic integral of first and second kind E and K respectively. For simplicity, $k^2$ is used for the expression:

$$k^2 = \frac{4ar\sin\theta}{a^2 + r^2 + 2ar\sin\theta} \tag{16}$$

We compare the analytical result of the vector potential with the result obtained by JOREK. JOREK calculates the value of the poloidal magnetic flux $\psi$ which is directly related to the toroidal component of the vector potential by:

$$RA_\varphi = \psi, \tag{17}$$

with R being the radial coordinate in the cylindrical system.

As we want to compare the vacuum fields, we have to set the computation parameters in a way that practically erases all plasma effects. The plasma current source is set to zero and the plasma pressure to a low value while the resistance is chosen very high in this test case. Therefore, there is practically no magnetic field created by the plasma and the result depends only on the coil field. When the current of the coil varies, a current is induced in the plasma shielding it from the coil field. At high resistance, the plasma response declines faster, so that the full penetration of the coil field is achieved in fewer time steps which means that the situation is close to vacuum conditions.

The coil is a current loop with a radius of 1 m facing the plasma and is placed at $x = 5\,m$ as it is shown in figure 3.8. The current is set to $1\,kA$ which produces

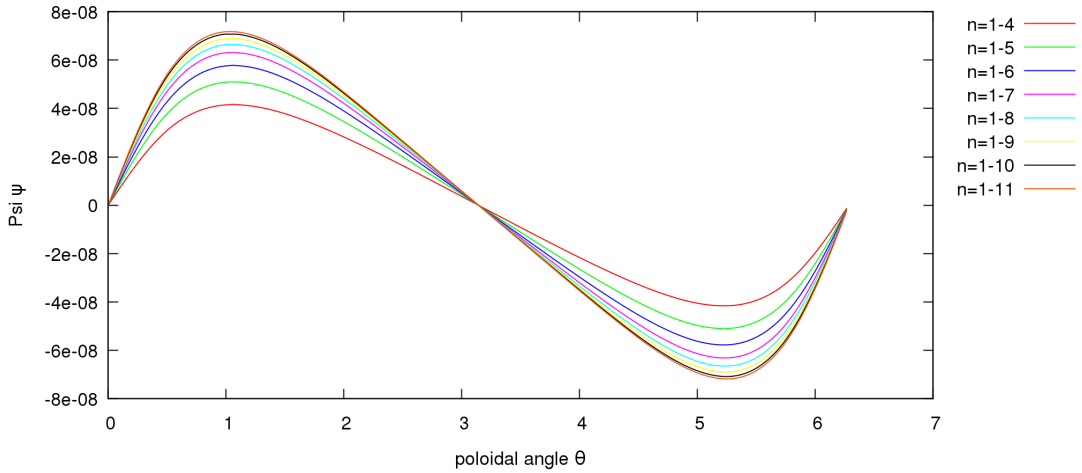


Figure 3.6: The goal of this test case is to compare the analytical value of the magnetic field with the value calculated by JOREK. A current loop that faces the plasma is located close to the plasma. The graphs show the poloidal magnetic flux on the plasma boundary in dependence of the poloidal angle in a tokamak with circular cross section. As the coil is not toroidally symmetric, many Fourier harmonics have to be considered to give a realistic result. Therefore, the number of harmonics was increased in the calculation to show that the value converges. (Own representation)

a magnetic field that is high enough to cover the remaining plasma effects. The JOREK field is calculated at the Gauss points on the boundary where we also evaluate equation (15) analytically. As the coil is not toroidally symmetric, a multitude of harmonics has to be taken into account to obtain a valid result. Figure 3.6 shows how the value of the magnetic flux converges to a certain value when sufficient toroidal harmonics are considered.

The comparison to the analytically calculated tangential magnetic field in figure 3.7 shows that qualitative shape is similar to the JOREK magnetic field, also the order of magnitude and the sign fit. However, the curvature and the amplitude of the vector field do not match. To find the reason for this problem, the simulation was repeated for different resolutions of the wall and the plasma as well as for changes of the plasma parameters like viscosity, diffusion and resistivity. All of these parameters turned out to be converged well enough that the result did not change considerably in the scans. Thus, the mismatch between the numerical and analytical value has to be resolved in future works.

We have seen that the magnetic field of the coils are close to the expected results. In the following section, a more elaborate test case is set up. The error field penetration of an RMP coil in JOREK-STARWALL is tested and compared to a previous implementation with fixed boundary conditions.

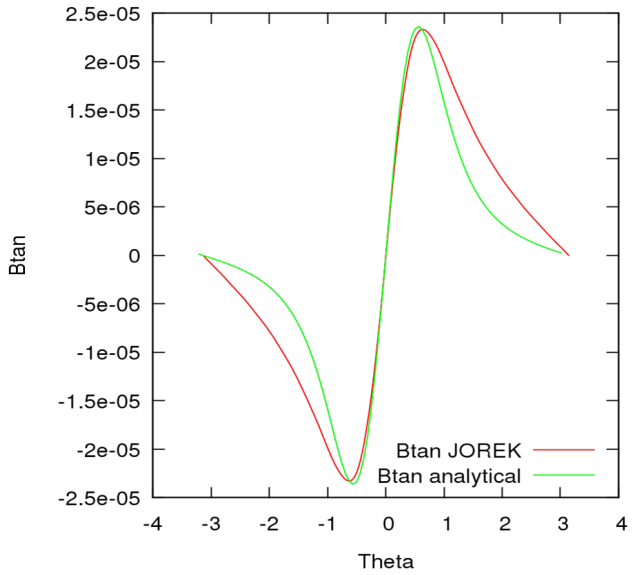


Figure 3.7: The comparison between the analytical and the JOREK value of the tangential field in the poloidal plane shows that the overall shape of the field is similar while the amplitude and location of the maximum do not correspond to the theoretical value. The analytical field was scaled with a factor of 0.8 to fit the JOREK data. This mismatch can be due to remaining unwanted plasma effects or due to an error in the computation which requires some additional analysis beyond the scope of this thesis. (Own representation)

## 3.6 RMP coil field penetration

The issue of ELMs and the importance of resonant magnetic perturbation (RMP) coils were introduced above in the sections 2.4 and 2.5. The last application of coils in this thesis is an ASDEX Upgrade case with 16 RMP coils. For this, the coordinates of the RMP coils were used for the STARWALL input which can be seen in figure 3.9 including the wall and the cross section of the plasma. Before the implementation of coils in STARWALL, the effect of the coils was calculated externally using a vacuum field assumption and imposed on JOREK as fixed perturbation at the plasma boundary (Dirichlet boundary conditions) as decribed in reference [Ora13]. With the changes to JOREK and STARWALL, the effects can be modelled more realistically by using natural boundary conditions.

Different from the simple test cases above, JOREK now takes into account so called neo-classical and diamagnetic effects (see reference [Ora13]) to obtain more realistic results which can then be compared to the experimental observations. First, the simulation is run axisymmetrically to make sure plasma flows can establish steady state. Afterwards, more harmonics are added and the RMP currents are ramped up to their final values in about 0.5 ms, similarly to how it is done in experiments as well as to prevent numerical instabilities. The current

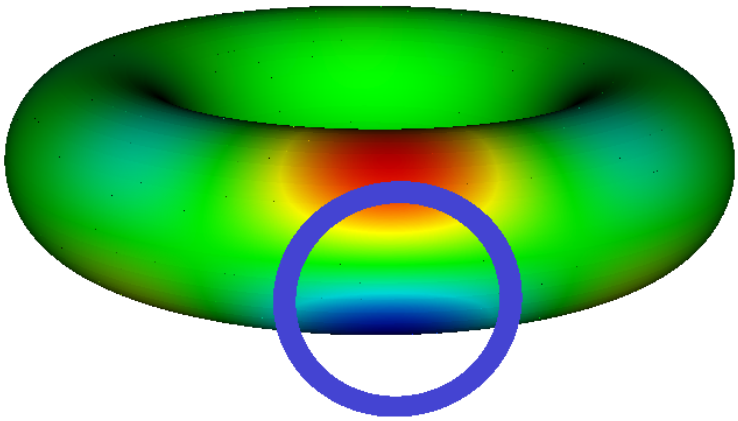

Figure 3.8: The coil is oriented towards the plasma at x=5 m. The plasma itself has a major radius of 3 m and the cross section a radius of 1 m. The magnetic flux that is produced by the coil has qualitatively the expected form and sign, only the magnitude does not exactly match the analytical field. The width of the coil was increased in this figure to make it disinguishable. (Own representation)

in every second coil is set to zero while the maximal amplitude of the other coils is 1.25 kA. The orientation of the current in the coil changes between two neighbouring coils with current. Each coil has 4 turns, so that the total current is 5 kA.

As described in section 2.5, the RMP coils create magnetic islands on resonant surfaces in the plasma which are characterised by a rational safety factor. When those islands grow large enough to overlap, they form an ergodic layer at the edge. The plasma response shields the plasma core from perturbations, so that mostly the edge is affected. As it can be seen in the Poincaré plot of the magnetic field in figure 3.10, the RMP coils in JOREK create magnetic islands as predicted by theory. In the beginning, the islands are small. But, while the current is being ramped up, the islands grow and a small ergodic zone is created near the edge, where there are dots instead of flux surfaces.

The next sign that the RMP coils are working correctly is the magnetic flux on the plasma that displays the penetration of the magnetic field of the RMPs at the plasma edge as it is shown in figure 3.11. The penetration of the magnetic field is at the position of the coils on the upper and lower side of the plasma. The form of the penetration is similar to the old implementation, but the penetration depth seems lower. When the energy of the perturbations were compared, the energy of the freeboundary implementation was lower than the one with fixed boundary conditions. To obtain the same energy, the current was increased by a factor of 12. A more detailed validation will be done in future work.

It remains to investigate the exact field strength of the coils to see whether this

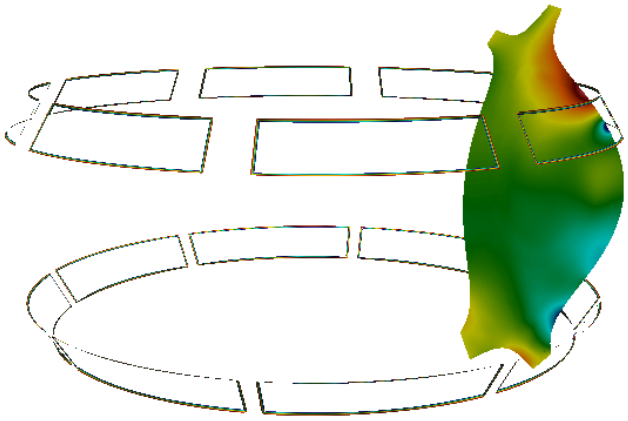

Figure 3.9: The coil configuration of AUG consists of 8 upper and 8 lower coils. A phase difference between the currents of the upper and the lower coil sets is often imposed to enhance the effects of the perturbation. After an axissymmetric calculation at the beginning, the coil currents are slowly ramped up to their final value. In experiments, this coil current can also vary with time, but at larger time scales than those considered in this test case. (Own representation)

result is fully correct. As shown in section 3.5, there might still be small problems in the implementation (e.g., a normalisation factor) but the implementation already gives qualitatively reasonable results even for the complicated case of 16 external RMP coils.

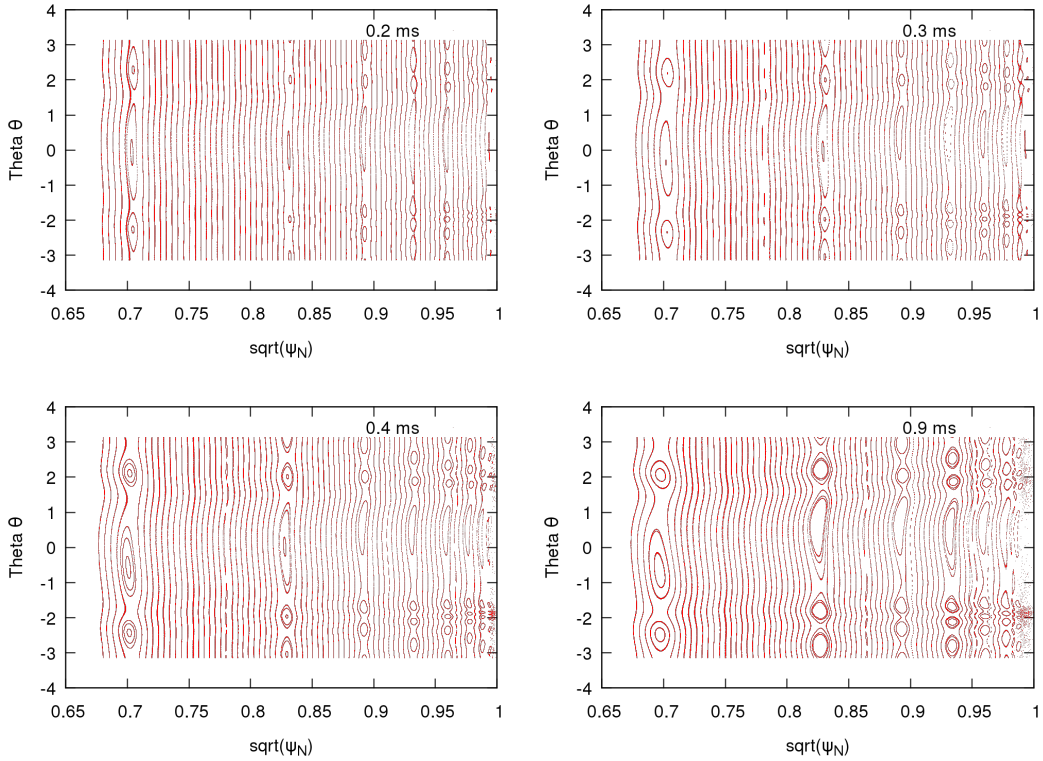


Figure 3.10: Poincaré plot of the magnetic field in the test case. The perturbation of the coils results in the creation of magnetic islands on resonant surfaces with a rational safety factor. When the magnetic perturbation is strong enough to form overlapping islands, an ergodic layer can be observed at the plasma edge. The figures represent the magnetic field lines from 0.2 to 0.9 ms after the start of the ramp up. At the beginning the current is not strong enough to form big islands. But when it is fully ramped up, larger islands are formed and a small ergodic zone is visible near the edge of the plasma. (Own representation)

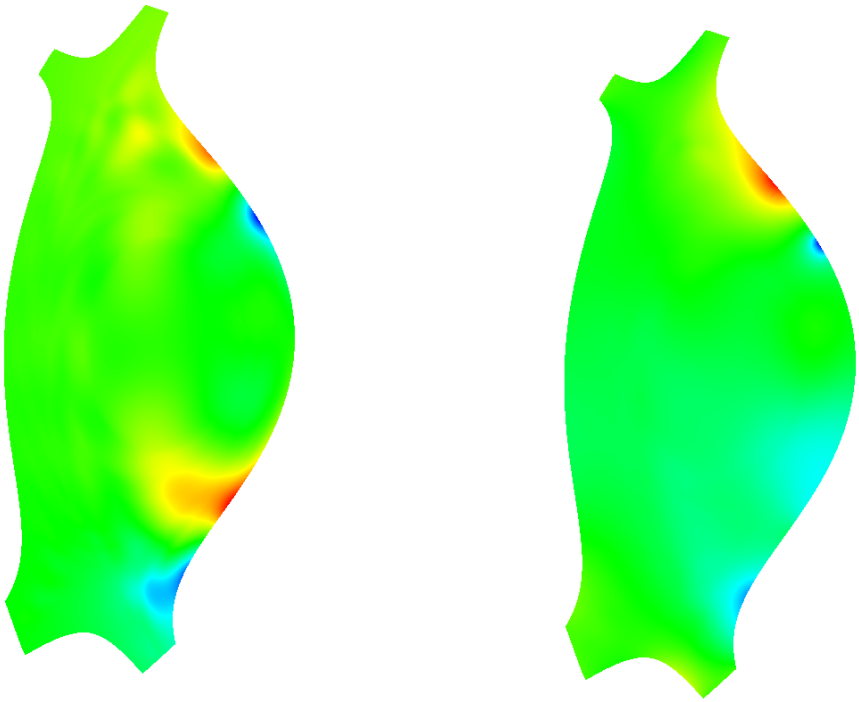

Figure 3.11: The magnetic flux perturbation on the plasma cross section clearly shows the effect of the RMP coils. The figure on the left shows the result of the fully penetrated RMP magnetic perturbation with the previous coil implementation, whereas the figure on the right shows the result of the RMP coils as calculated with STARWALL. At the edge, the penetration of the magnetic field is seen at the position of the upper and lower coils. (Own representation)

# 4 Conclusion and final remarks

The tasks of this thesis were to contribute to the implementation of coils in JOREK-STARWALL, to the validation of the model, and to make first applications with those coils.

The implementation of coils in STARWALL was mostly successful. The visualisation of the coils suggests that the discretisation of the coils into triangles works as intended and the computation of the STARWALL response is correct. The benchmark with CASTOR, where a wall without coils was considered, proved that the extended STARWALL version for coils gives the same growth rates. This shows that JOREK-STARWALL is working correctly.

The implementation in JOREK was largely completed. JOREK is now able to handle the coil input of STARWALL, take into account the boundary conditions given by STARWALL and visualise the coils with their current. An easy method for the description of the coil current time traces still needs to be implemented.

First, it was shown that interaction between several coils works correctly. Second, the plasma coil interaction was looked at. We saw that the magnetic flux of the coils is very close but does not fit perfectly to the analytical value. Therefore, it still remains to investigate whether it is a computational problem, or if the test case was not working correctly. In particular, there might be a normalisation problem as the value of the magnetic field is lower than the analytically calculated one.

Finally, the main goal for the implementation of coils in JOREK was to represent RMP coils more realistically as their role for the control of Edge Localized Modes is an important factor for future tokamaks like ITER. The first tests of RMP coils with the extended STARWALL version suggest that the magnetic field perturbation is qualitatively as expected. The comparison to the old handling of the coil field shows that the magnetic field penetration is similar and the growth rates are comparable. However, there might be a normalisation problem in the code which needs to be investigated. Future work will involve more extensive benchmarking tests to prove the consistency of the new implementation and the comparison to experimental results.

# Acknowledgements

I would like to thank IPP for giving me the opportunity and resources to complete my bachelor thesis. Especially, I would like to thank my supervisor Dr. Matthias Hölzl for his great support, many explanations, time for discussions and answering loads of questions. Dr. François Orain, for his explanations, literature recommendations and help with the RMP case.
Also, professor Heiko Rieger of the Saarland University for agreeing to be the supervisor of my home university.

# References


[AS17] Artola Such, J. Non-linear MHD simulations of ELM triggering via Vertical Kicks with JOREK-STARWALL. In *16th International Workshop on Plasma Edge Theory in Fusion Devices*. September 2017.

[Boy03] Boyd, T. J. M. and Sanderson, J. J. *The Physics of Plasmas*. Cambridge University Press, Cambridge, 2003. ISBN 978-0-521-45912-9.

[Che15] Chen, F. F. *Introduction to Plasma Physics and Controlled Fusion*. Springer, 2015. ISBN 978-3319223087.

[Cza08] Czarny, O. and Huysmans, G. Bézier surfaces and finite elements for MHD simulations. *Journal of Computational Physics*, 227(16):7423–7445, August 2008. ISSN 0021-9991. doi:10.1016/j.jcp.2008.04.001.

[Dol13] Dolan, T. J. (editor). *Magnetic Fusion Technology*, volume 19 2013 of *Lecture Notes in Energy*. Springer Science & Business Media, Berlin Heidelberg, 2013. ISBN 978-1-447-15556-0.

[Eva04] Evans, T. E., Moyer, R. A., Thomas, P. R., et al. Suppression of large edge-localized modes in high-confinement DIII-D plasmas with a stochastic magnetic boundary. *Physical Review Letters*, 92:235003, Jun 2004. doi:10.1103/PhysRevLett.92.235003.

[Fra15] Franck, E., Hölzl, M., Lessig, A., and Sonnendrücker, E. Energy conservation and numerical stability for the reduced MHD models of the non-linear JOREK code. *ESAIM: Mathematical Modelling and Numerical Analysis*, 49(5):1331–1365, 2015.

[Hav16] Haverkort, J. W., de Blank, H. J., Huysmans, G. T. A., Pratt, J., and Koren, B. Implementation of the full viscoresistive magnetohydrodynamic equations in a nonlinear finite element code. *Journal of Computational Physics*, 316:281–302, July 2016. doi:10.1016/j.jcp.2016.04.007.

[Hoe12] Hoelzl, M., Merkel, P., Huysmans, G. T. A., et al. Coupling JOREK and STARWALL codes for non-linear resistive-wall simulations. *Journal of Physics: Conference Series*, 401(1):012010, 2012. doi:10.1088/1742-6596/401/1/012010.

[Huy07] Huysmans, G. and Czarny, O. MHD stability in X-point geometry: simulation of ELMs. *Nuclear Fusion*, 47(7):659, 2007. doi:10.1088/0029-5515/47/7/016.

[Igo14] Igochine, V. (editor). *Active Control of Magneto-hydrodynamic Instabilities in Hot Plasmas*. Springer, Berlin, Heidelberg, 2015 edition, 2014. ISBN 978-3-662-44222-7.

[ITE] URL `www.iter.org`. Last retrieved 18.04.2017.

[Lan13] Lang, P., Loarte, A., Saibene, G., et al. ELM control strategies and tools: status and potential for ITER. *Nuclear Fusion*, 53(4):043004, Jun 2013. doi:10.1088/0029-5515/53/4/043004.

[Lia10] Liang, Y., Koslowski, H.-R., Jachmich, S., et al. Overview of ELM Control by Low n Magnetic Perturbations on JET. *Plasma and Fusion Research*, 5:S2018, 2010. doi:10.1585/pfr.5.S2018.

[Mer15] Merkel, P. and Strumberger, E. Linear MHD stability studies with the STARWALL code. *arXiv*, 2015. URL https://arxiv.org/abs/1508.04911.

[Min] Mink, F., Hoelzl, M., Wolfrum, E., et al. Nonlinear coupling induced toroidal structure of Edge Localized Modes. Submitted.

[Min16] Mink, F., Wolfrum, E., Maraschek, M., et al. Toroidal mode number determination of ELM associated phenomena on ASDEX Upgrade. *Plasma Physics and Controlled Fusion*, 58(12):125013, 2016.

[Miy06] Miyamoto, K. *Plasma Physics and Controlled Nuclear Fusion*. Springer Science & Business Media, Berlin Heidelberg, 1. edition, 2006. ISBN 978-3-540-28097-2.

[Ora13] Orain, F., Bécoulet, M., Dif-Pradalier, G., et al. Non-linear magnetohydrodynamic modeling of plasma response to resonant magnetic perturbations. *Physics of Plasmas*, 20(10):102510, 2013. doi:10.1063/1.4824820.

[Ora17] Orain, F., Hölzl, M., Viezzer, E., et al. Non-linear modeling of the plasma response to rmps in ASDEX Upgrade. *Nuclear Fusion*, 57(2):022013, 2017. doi:10.1088/0029-5515/57/2/022013.

[Sim01] Simpson, J. C., Lane, J. E., Immer, C. D., Youngquist, R. C., and Steinrock, T. Simple analytic expressions for the magnetic field of a circular current loop. Technical report, NASA, 2001.

[Sut11] Suttrop, W., Eich, T., Fuchs, J. C., et al. First observation of Edge Localized Modes mitigation with resonant and nonresonant magnetic perturbations in ASDEX Upgrade. *Physical Review Letters*, 106:225004, Jun 2011. doi:10.1103/PhysRevLett.106.225004.

[Wes11] Wesson, J. *Tokamaks*. OUP Oxford, New York, London, 4th edition, 2011. ISBN 978-0-199-59223-4.

[Zoh96] Zohm, H. Edge Localized Modes (ELMs). *Plasma Physics and Controlled Fusion*, 38(2):105, 1996. doi:10.1088/0741-3335/38/2/001.